Photo-thermo-mechanically actuated liquid crystalline elastomer nanocomposite reinforced by polyurethane fiber-network

Wanqiu Zou, Xuezhen Huang, Qingkun Li, Licheng Guo, Chensha Li & Hongrui Jiang

Published online: 12 Jul 2016.

Submit your article to this journal

Article views: 29

View related articles

View Crossmark data

Taylor & Francis
Taylor & Francis Group

Photo-thermo-mechanically actuated liquid crystalline elastomer nanocomposite reinforced by polyurethane fiber-network

Wanqiu Zou[a,†], Xuezhen Huang[b], Qingkun Li[c], Licheng Guo[a], Chensha Li[d], and Hongrui Jiang[b,e]

[a]Department of Astronautic Science and Mechanics, Harbin Institute of Technology, Harbin, China; [b]Department of Electrical and Computer Engineering, University of Wisconsin-Madison, Madison, WI, USA; [c]Department of Electronic Engineering, Heilongjiang University, Harbin, China; [d]Key Laboratory of Functional Inorganic Material Chemistry, Ministry of Education, Heilongjiang University, Harbin, China; [e]Materials Science Program, University of Wisconsin-Madison, Madison, WI, USA

ABSTRACT

In this work, we develop a nanocomposite consisting of nematic liquid crystal elastomer (LCE) matrix incorporated with single-wall carbon nanotubes (SWCNTs) and the reinforcement phase of polyurethane fiber-network (PUFN). The photo-thermo-mechanical actuation of LCE matrix is realized by converting light into heat with assistant of SWCNTs. The PUFN enhances the mechanical properties of the material, thus the actuation capability. Under the irradiation from a wide-spectrum light source with an intensity on the order of 100 mW/cm^2, the PUFNs/SWCNT/LCE nanocomposite contracts up to 27% of the original length in several seconds due to the photo-induced strain, and recovers to the original length in several seconds after the light source is switched off. The efficiency of actuation is not light-spectrum dependent. The maximum effective actuation force is about 260 kPa, much larger than that of the LCE material without the reinforcement of PUFNs. The tensile strength and the performance of anti-fatigue failure under multiple reversible actuations are also greatly improved. The mechanism of the actuation capability of LCE material involved in the fiber-network reinforcement phase is studied.

1. Introduction

There has been considerable effort to develop human made actuator materials, which can exhibit effective mechanical actuation induced by external stimuli such as electric field, temperature, and light. Actuator materials with different characteristics and mechanisms have been widely adopted in industry for a variety of demands [1–5]. Liquid-crystalline elastomers (LCEs) have attracted much attention over the past twenty years due to their exceptional properties different from other high-molecular-weight polymers. They possess both anisotropic orientational symmetry and sparsely cross-linked rubbery network of flexible polymers, thus complex mechanical behaviors because of the couple of the orientational degrees of freedom

---

CONTACT Licheng Guo ✉ guolc@hit.edu.cn; Chensha Li ✉ lichnsa@mail.tsinghua.edu.cn; Hongrui Jiang ✉ hongrui@engr.wisc.edu

Color versions of one or more of the figures in the article can be found online at www.tandfonline.com/gmcl.

†Wanqiu Zou, Xuezhen Huang and Qingkun Li contributed equally to this work.

of liquid crystalline order and those of rubber-elastic matrix [6–11]. One of the most outstanding features of nematic LCEs is a equilibrium reversible change in shape that is different from other shape-memory materials which act only in a one-stroke way and require a reset after every actuation.

Light-induced LCE actuators have been developed and utilized as swimming motion [12], cilia motion [13], oscillators [14], motor [15], microrobots [16], micropumps [17], microvalves [18], hinges [19], and optical pendulum generator [20]. Nowadays the optical actuation of nematic LCEs are performed mainly by two ways: one is incorporating photoisomerizable molecules or molecular chromophores into the LCE network; the shape change of the photoisomerizable molecules or molecular chromophores driven by light can cause deformation of host materials [7, 8, 12–18, 20–25]. This type of LCE materials can only be actuated by the lights with specific wave-lengths. Another way is based on photo-thermo-mechanical actuation, including two sub-ways: one is incorporating photoresponsive dye molecules into LCE matrices [19]. The incorporated dye molecules can absorb some spectral spectrum of IR to create vibrations. These vibrations of dye molecules or molecular groups create thermal energy in LCE matrices, elevating the temperature to above the nematic–isotropic transition temperature (T_{ni}), changing the nematic order, and leading to the strain and mechanical actuation. This type of LCE materials can also be actuated by the wavelength-selective lights. Another sub-way is incorporating nano-phase materials, such as carbon nanotubes (CNTs), which possess high photo-thermal conversion efficiency and thermal conductivities, into LCE matrices. The incorporated nano-phase materials can efficiently absorb and transform photo energy into thermal energy, and serve as a nanoscale heat source and thermal conduction pathway to heat the matrices effectively, elevating their temperature to above the T_{ni}, and resulting in the shape-changing and mechanical actuation of LCE materials [26–30]. This type of LCE materials is capable of utilizing the photon energy of wide spectrum to realize opto-thermo-mechanical actuation, which increases their adaptability to various light sources, and even the natural sun light [30]. However, due to their limited mechanical properties, such as they are prone to fracture during the actuation process under a high temperature and a high actuation loading [30, 31], which limits their application as actuator materials.

A major method of enhancing the mechanical properties of polymer materials is incorporating the reinforcement phase into the polymer matrices [32]. It was reported that adding CNTs into the LCE matrices could improve their mechanical properties [26, 28, 33, 34]. In principle, their mechanical performances should be much enhanced with the reinforcement of continuous phase materials [32]. Other researchers developed LCE composites with laminated structure composed of a LCE and a flexible polymer substrate, thereby mechanical strength could be improved with the polymer substrate. LCE composites with this laminated structure can only perform asymmetric deformations [35, 36], such as bending or distortion, due to nonuniform strain through the laminations. By incorporating a continuous fiber into LCE as the reinforcement phase, we developed a photo-thermo-mechanically actuated LCE nanocomposite with a LCE contained single-wall carbon nanotubes (SWCNTs) as the matrix and polyurethane fiber-network (PUFNs) as the reinforcement phase [30]. The contained SWCNTs performed absorbing and transforming photo energy into thermal energy to drive the actuation of LCE matrix; the incorporated PUFNs performed mechanical reinforcement of the material while not influenced its symmetric deformation during the actuation process. The PUFNs/SWCNT/LCE nanocomposite behaved larger actuation capability as a photo-thermo-mechanical actuator compared to the LCE materials without the reinforcement of continuous phase materials, and demonstrated superior performances in

engineering application [30]. In this work, the performances of photo-thermo-mechanical actuation were further studied.

2. Experimental procedures

2.1 Materials preparation

The pendant mesogenic group: 4-methoxyphenyl-4-(1-buteneoxy) benzoate. Di-functional crosslinking group: 1, 4 alkeneoxybenzene, were synthesized as our work reported in ref. [28]. The polymer backbone was a poly-dimethylhydrosiloxane (PMHS) with approximately 60 Si–H units per chain, obtained from ACROS Chemicals (Belgium, USA). The commercial platinum catalyst, dichloro(1, 5-cyclooctadiene) platinum(II), was obtained from Aldrich (St Louis, USA). The synthesis and fabrication of PUFN/SWCNT/LCE nanocomposite was same as reported in ref. [30].

2.2 Characterization methods

The LCE mesomorphic properties were observed using polarizing optical microscopy (Nikon Instruments, SMZ 1500, Melville, NY). X-ray diffraction spectra were measured by a Bruker/Siemens Hi-Star 2 d X-ray Diffractometer with a monochromatic CuKalpha point source (0.8 mm). The photoactuation measurements were performed by using a wide-spectrum light source (New Port, Oriel Productline, Model 66885, Irvine, CA). The phase transformation behavior was investigated by differential scanning calorimetry (DSC) measurements (TA Instruments Q100 modulated differential scanning calorimeter, New Castle, DE) at a heating and cooling rate of 10 K min^{-1}. The temperature change of the films in response to the light stimulus was tested by a multilogger thermometer (HH 506 RA, OMEGA Engineering, Stamford, CT). The detector, with the dimension of 2 mm in length and 100 μm in diameter, was placed on the sample surfaces. A stress meter was employed to measure the retractive forces of the LCE materials during photo actuation and their tensile strength. The environment temperature of experiments was 25°C. A finite unit software "ABAQUS" was used to simulate the stress distribution in the LCE materials.

3. Results and discussions

The PUFN, with a thickness of 0.3 mm to 0.4 mm, was used to reinforce the LCE matrix. Fig. 1 (a), a micrograph image of the used PUFN, demonstrates that the PUFN was a network structure constructed by polyurethane fibers ∼70 μm in diameter. The pores in the network were irregular with the size of 0.3 mm to 0.5 mm. The X-ray diffraction pattern of PUFN shows a bright ring with uniform intensity (Fig. 1(b)), corresponding to a isotropic molecule structure. The LCE nanocomposites with PUFN reinforcement phase were in situ synthesized through a two-stage crosslinking coupled with a drawing process. To avoid the aggregation of CNTs and enable the incorporation of PUFN into LCE matrix during the synthesis of LCE, the generally used centrifugation and heating processes for the first crosslinking stage [6] was substituted by molded casting and heating [30], the PUFN did not react to the components of the synthesis system due to its chemistry inertness. Moreover, the highly flexible PUFN could freely compressed or stretched together with the LCE matrix during the fabrication process and the actuated shape-changing process under the applied stimuli, without hindrance on
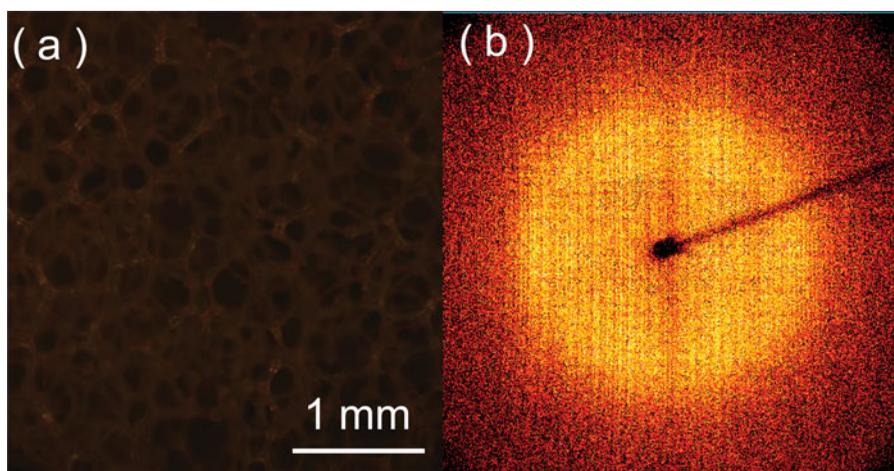
Figure 1. (a) A optical micrographs of the PUFN. (b) The X-ray diffraction pattern of the bare PUFN.

the alignment of the mesogens. In order to evaluate the anisotropic alignment of the mesogens in the LCE matrix of the composite, we first measured the transmittance of a probe light through two crossed polarizers with a PUFN/LCE composite film, fabricated using the same process of PUFN/SWCNT/LCE nanocomposite but without SWCNTs, between them. The polarizing optical micrographs (POMs) are shown in Fig. 2. Though the PUFN blocked part of the light, it still demonstrated that the highest transmittance appeared when the angle between the stretch direction of the film and the polarization direction of either polarizer was 45°, while the lowest appeared when the stretch direction was parallel to one of the polarization directions. Periodic changes of dark and bright images were observed by rotating the film with an interval of 45°. The result confirmed an LCE nematic-phase, and that the mesogenic units were well aligned along the stretch direction. The POM measurement of the SWCNT/LCE nanocomposite films, which were fabricated as the same process of PUFN/SWCNT/LCE nanocomposite but without PUFN, demonstrated consistent results [28]. For the PUFN/SWCNT/LCE nanocomposite, due to the serious blocking of light by the PUFN and the SWCNTs dispersed in LCE, the transmittances in the images were too weak to be observed. The anisotropic alignment of the mesogens in LCE matrix
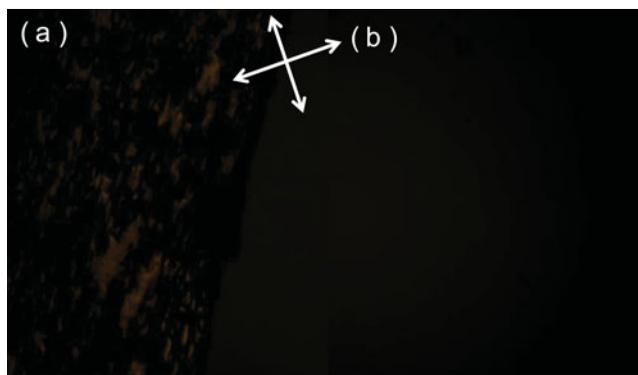
Figure 2. Polarizing optical micrographs (POM) of the PUFN/LCE composite film. (a) The angle between the stretch direction of the film and the polarization direction of either polarizer is 45°. (b) The stretch direction of the film is parallel to one of the polarization direction. The crossed arrows is the orientations of the crossed polarizers.
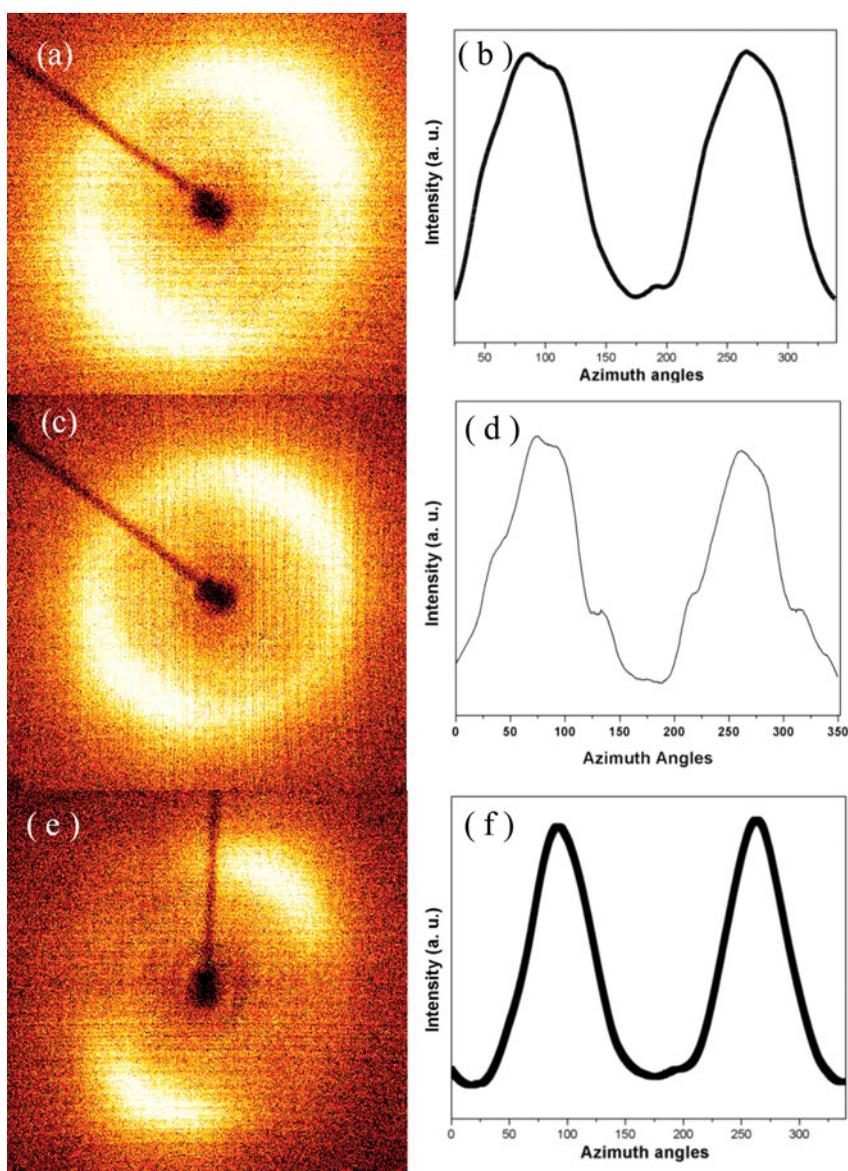
Figure 3. (a) An X-ray diffraction pattern obtained from a PUFN/SWCNT/LCE sample. (b) Azimuthal intensity distribution of the X-ray diffraction pattern of PUFN/SWCNT/LCE. (c) An X-ray diffraction pattern obtained from a PUFN/LCE sample. (d) Azimuthal intensity distribution of the X-ray diffraction pattern of PUFN/LCE. (e) An X-ray diffraction pattern obtained from SWCNT/LCE sample. (f) Azimuthal intensity distribution of the X-ray diffraction pattern of SWCNT/LCE.

of the PUFN/SWCNT/LCE nanocomposite was investigated using X-ray scattering. Fig. 3 (a) exhibits a characteristic X-ray diffraction pattern of an aligned nematic liquid crystal [37] with a pronounced azimuthal distribution of intensity at $2\theta = 20.15°$, corresponding to a dimension of lateral packing mesogenic units ~ 0.46 nm. Comparing Fig. 3 (a), (c), and (e), it can be found that the X-ray diffraction pattern of PUFN/SWCNT/LCE nanocomposite was consistent with that of the PUFN/LCE composite and SWCNT/LCE nanocomposite, but the introduction of PUFN in nematic LCE matrix brought a broad ring in the X-ray diffraction pattern, as shown in Fig. 3 (a) and (c). The uniaxially ordered LCE matrix created two high

intensity areas of diffraction, corresponding to the two peaks in the azimuthal integration of wide-angle diffraction arc, as shown in Fig. 3 (b), (d), and (f). Some smectic fluctuations can brought weak small angle reflections on the equator in the X-ray diffraction pattern [37], which resulted in the weak shoulder peaks between two large peaks in Fig. 3 (b), (d), and (f).

Experiments demonstrated that our SWCNT/LCE nanocomposites could be reversibly actuated by the light with wide-spectrum [28], and the photo-induced actuation characteristic of the PUFN/SWCNT/LCE nanocomposite was consistent with that of SWCNT/LCE nanocomposites. Being exposed to 230 mW/cm^2 photo irradiation of white light, the PUFN/SWCNT/LCE nanocomposite film started conspicuous contraction and reached maximum contraction during 12 seconds, as shown in Fig. 4. The maximum contraction ratio was about 27%. It recovered to its initial length 12 seconds after the light source was switched
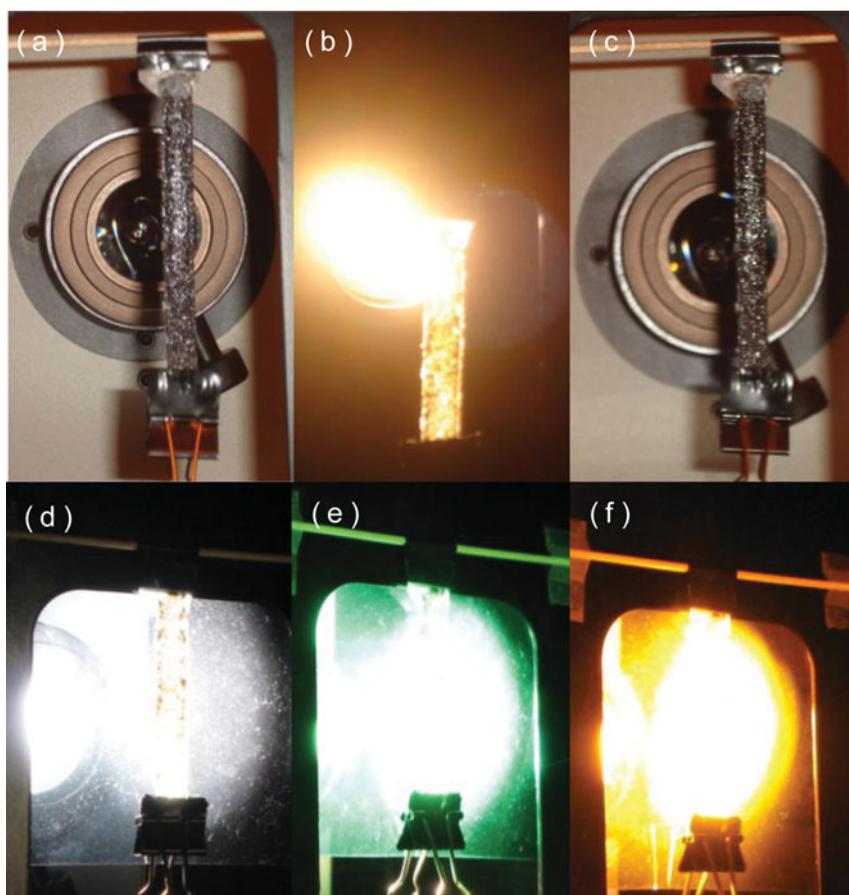
Figure 4. (a–c) Optical images of the photo-actuation of a PUFN/SWCNT/LCE film. The film, with a dimension of 83 mm × 12 mm × 0.8 mm and a load of 3 g weight, is irradiated by an incident white light of 230 mW/cm^2: (a) The initial state of the PUFN/SWCNT/LCE film. (b) It contracted to a stable length of 60 mm, which was about 27% of the initial length, after ∼12 seconds under irradiation. (c) It recovered to its initial length ∼12 seconds after the light source was switched off; (d–f) Optical images of the photo-actuation of the PUFN/SWCNT/LCE film irradiated by the filtered light with the intensity of 230 mW/cm^2: (d) Irradiated by the light filtered to the spectrum ranged from 380 nm to 500 nm. (e) Irradiated by the light filtered to the spectrum ranged from 480 nm to 580 nm. (f) Irradiated by the light filtered to the spectrum ranged from 580 nm to 720 nm. Under every irradiation of different spectrum, it contracted to the stable length of about 27% of the initial length.

off, indicating completely reversible photo-actuation. Temperature measurement demonstrated that the temperature of PUFN/SWCNT/LCE nanocomposite film increased to about 85°C at its maximum contraction under photo irradiation, which is above the T_{ni}, 68°C measured using DSC [30]. We further measured the photo-actuation performance of the PUFN/SWCNT/LCE nanocomposite by the lights of different spectrum ranges. The emitted white light was filtered to be different limited wavelength ranges by three optical filters, respectively, the wavelength ranges of the transmitted lights selected were 380 ∼ 500 nm, 480 ∼ 580 nm and 580 ∼ 720 nm. The PUFN/SWCNT/LCE nanocomposite demonstrated the consistent photo-actuation performance when it was irradiated by the lights with varied wavelength ranges but the same intensity, as shown in Fig. 4, which indicated that the efficiency of photo-actuation has no spectral spectrum dependence. The photo-actuation of the SWCNT/LCE nanocomposite also didn't show any dependence to these light wavelengthes. Therefore, the LCE nanocomposites, fabricated by incorporating SWCNTs into this LCE matrix, fully utilized the photo-energy from a wide-spectrum light source, such as sunlight [30], for mechanical actuation. However, the PUFN/LCE composite could not be actuated by wide-spectrum visible lights though it could be thermally actuated, as the blank LCE [28]. This indicated that PUFN embedded in the LCE matrix didn't contribute to the transformation of light to heat for the actuation of LCE.

As mentioned above, this axial contraction was due to the change of orientational order during the nematic-isotropic transition. With the orientational order decreasing, the conformational constraint on the LCE network was overcome, and it then can change shape and generate a retractive force, namely mechanical actuation. The maximum axial contraction ratio of PUFN/SWCNT/LCE nanocomposites after nematic-isotropic transition decreased as the loading was increased during the opto-thermal-mechanical actuation process, as shown in Fig. 5. It can be attributed to the larger loading-induced stretching strain of the material. If both ends of LCE composite were fixed, the film could not shrink under irradiation, and then the maximum retractive force of the elastomer could be measured under such a condition. The measured maximum retractive force of the PUFN/SWCNT/LCE nanocomposite caused by opto-thermal-mechanical actuation was 263 kPa, which was the maximum load-actuation, as shown in Fig. 5. However, the SWCNT/LCE nanocomposite, without the reinforcement of PUFN, was generally fractured during opto-thermal-mechanical actuation process when its loading was above 145 kPa. This meant that the effective load-actuation
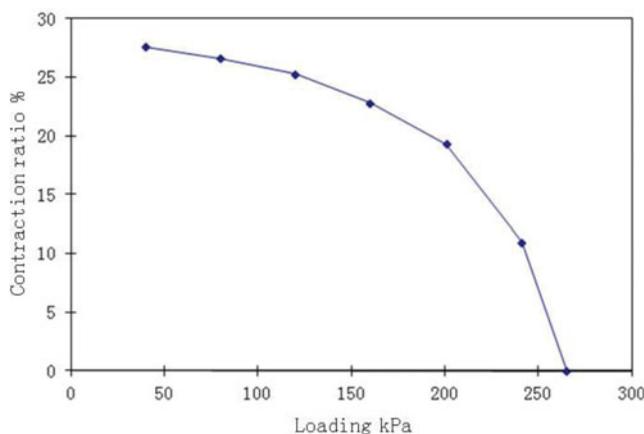
Figure 5. Maximum axial contraction ratio under opto-thermal-mechanical actuation of PUFN/SWCNT/LCE nanocomposite with varied loading.
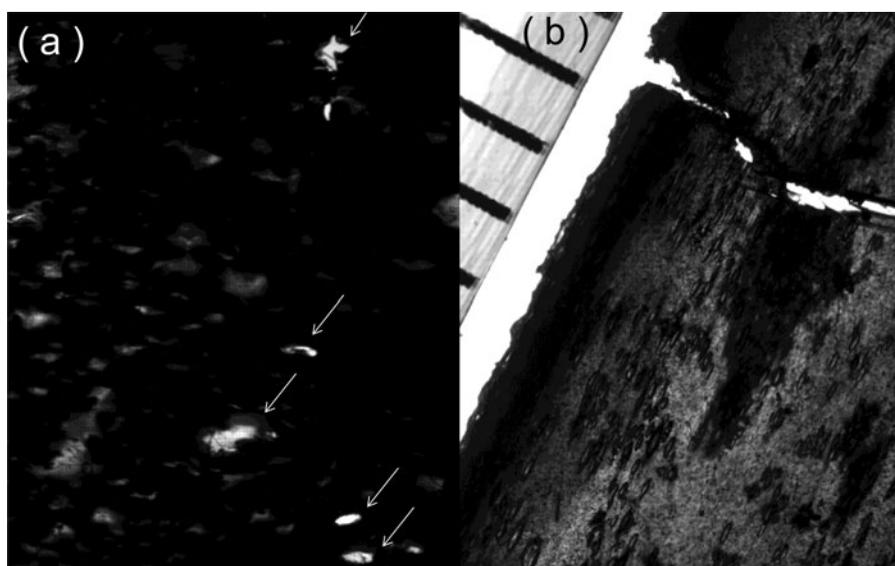
Figure 6. (a) A optical micrograph of a PUFN/SWCNT/LCE nanocomposite which was tested by repeated tensile fracture. The bright parts pointed by arrows are the tiny cracks in LCE matrix whose expansion was restricted by the polyurethane fibers. (b) A optical micrograph of a SWCNT/LCE nanocomposite which was tested by repeated tensile fracture. The cracks in LCE matrix expanded unrestrictedly.

capability of SWCNT/LCE nanocomposite was below 145 kPa, which was far lower than the maximum retractive force of PUFN/SWCNT/LCE nanocomposite. This fracture of the LCE materials could be associated with the fine defects in LCE matrix, which might be derived from the tiny voids inside the LCE matrix, the mini cracks on the edges created during the contraction process or the mini cracks caused by local stress concentration. Under a higher temperature and load, the fine defects in LCE matrix tended to be expanded, especially at some areas with concentrated stresses, such as the area fixed by clamps, and led to the fracture. Thus it might be observed that the LCE materials were fractured before their retractive forces arrived at the maximum values during the actuation process [31]. For the PUFN/SWCNT/LCE nanocomposite, the incorporated PUFN could effectively inhibit the expansion of the defects in LCE matrix and elevated the robustness of the material, thereby the effective load-actuation capacity was greatly increased. Fig. 6 shows the optical micrographs of a PUFN/SWCNT/LCE nanocomposite and a SWCNT/LCE nanocomposite which were tested by repeated tensile fracture. It clearly shows that the cracks in LCE matrix of the PUFN/SWCNT/LCE nanocomposite were restricted by the polyurethane fibers, but the cracks in SWCNT/LCE nanocomposite extended unrestrictedly.

The tests on tensile strength, as shown in Fig, 7, indicated that the tensile strengths of the PUFN/SWCNT/LCE nanocomposite and the SWCNT/LCE nanocomposite were similar at room temperature. But the tensile strength of the PUFN/SWCNT/LCE nanocomposite at the temperature around its T_{ni} was measured to be around 800 kPa, much higher than the maximum retractive force during nematic-isotropic transition, while that of the SWCNT/LCE under the same condition was about 160 kPa, lower than the maximum retractive force during nematic-isotropic transition. The reason lies in that the mechanical property of PUFN was attenuated much lower than that of the LCE matrix as the temperature increased from room temperature to T_{ni}, thus the material was still effectively reinforced by the incorporated PUFN
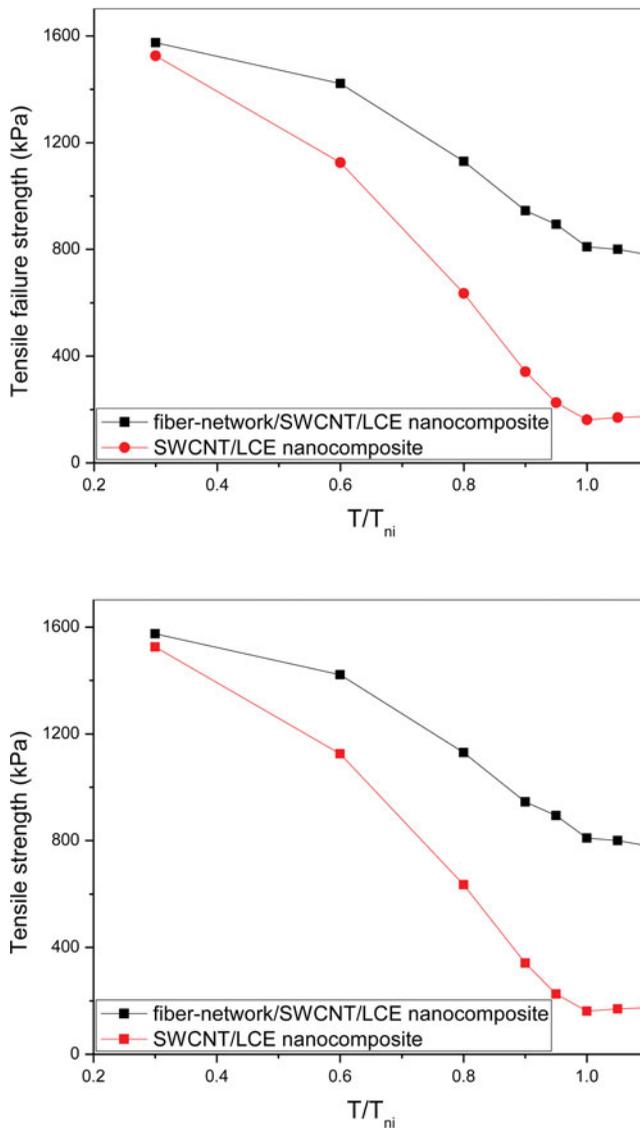
Figure 7. The tensile strengths of the PUFN/SWCNT/LCE nanocomposite and the SWCNT/LCE nanocomposite at different reduced temperature (T/T_{ni}).

at a high temperature around the T_{ni}. Therefore, in opto-thermal-mechanical actuation processes, the PUFN/SWCNT/LCE nanocomposite could not be fractured by its retractive force. The effective load-actuation capability could be up to its maximum retractive force. By contrast, the SWCNT/LCE nanocomposite still fractured even if its loading was lower than the maximum retractive force due to its lower effective load-actuation capability than the maximum retractive force.

In addition, the incorporated PUFN undertook part of the stresses and dispersed the stresses evenly in the LCE matrix during the mechanical actuation process of the LCE nanocomposite, thus could reduce the local stress concentrations, which might cause the local damages in LCE matrix. We employed software simulation utilizing "ABAQUS" to analyze the stress distribution in the LCE materials. Here we utilized a model by fixing the LCE materials
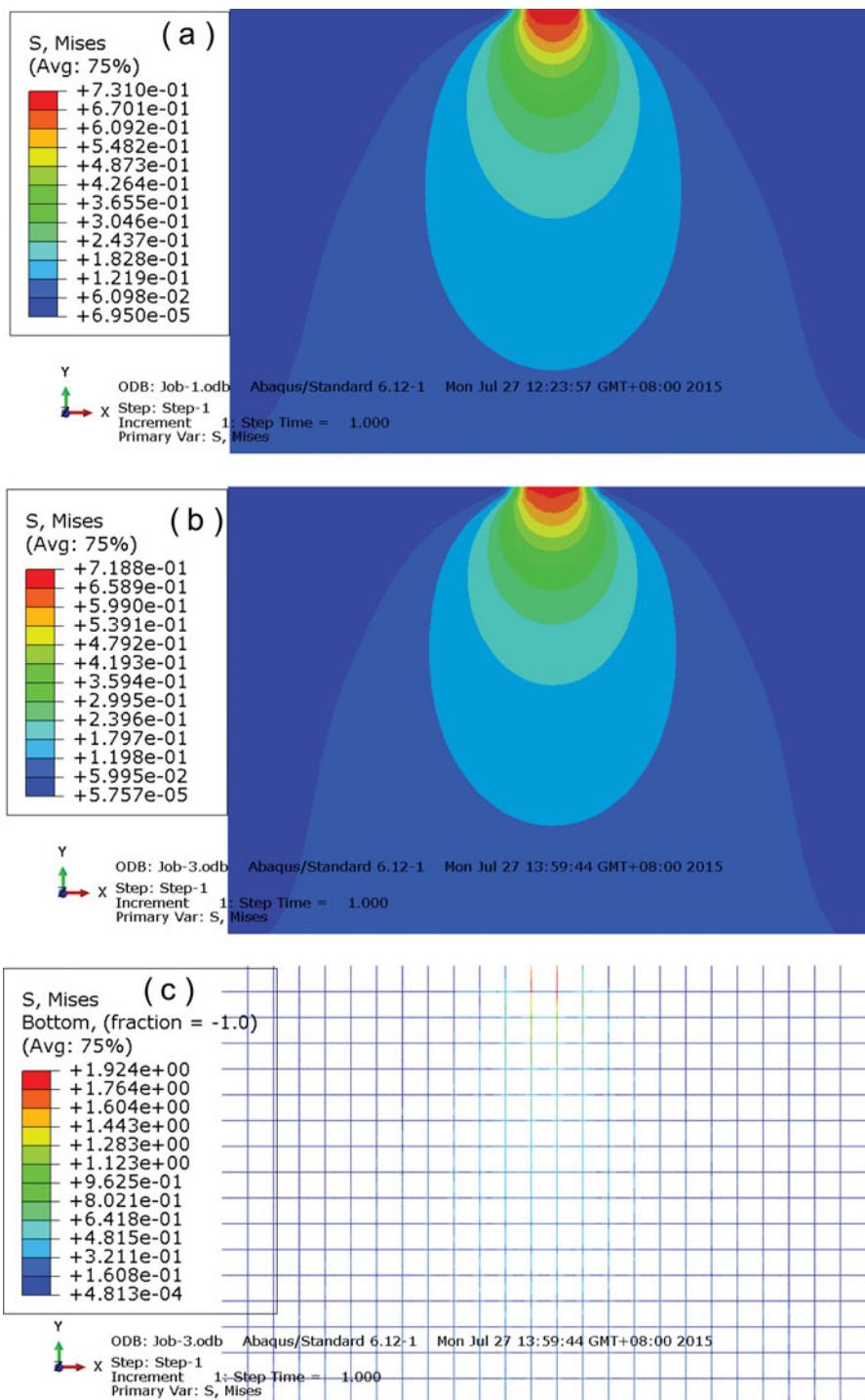
Figure 8. The stress distribution in LCE material when the material is drawn at the middle part of one end while the other end is fixed. (a) The stress distribution in LCE matrix for the SWCNT/LCE nanocomposite. (b) The stress distribution in LCE matrix for the PUFN/SWCNT/LCE nanocomposite. (c) The stress distribution in PUFN for the PUFN/SWCNT/LCE nanocomposite. The drawing force is 800 kPa. The reduced temperature (T/T_{ni}) is 0.9.

at one end and drawing the middle part of the other end, and comparing the stress distribution with and without the PUFN as reinforcement phase. As shown in Fig. 8, the area of high stress in LCE matrix incorporated with PUFN is obviously less than that without PUFN, while the PUFN undertakes part of stresses. This study means that the incorporated PUFN could effectively disperse the stress undertaken by LCE material and overcome the local stress concentrations which might create the local damages in LCE matrix. This should be one of the reasons why the PUFN/SWCNT/LCE nanocomposite had high capabilities of actuation, anti-failure and anti-environment influence during the stimuli actuation process.

Experiment of anti-fatigue failure under multiple reversible photo actuation demonstrated that for the SWCNT/LCE nanocomposite with a loading of 75 kPa, the cycle number of continuously reversible photo actuation without fatigue fracture was generally lower than 20 times. While the PUFN/SWCNT/LCE nanocomposite could not be damaged after above 100 cycles of continuously reversible photo actuation with the same loading. These superior performances of PUFN/SWCNT/LCE nanocomposites enable them to be applied in engineering area.

4. Conclusions

Among various materials used in actuator designs, the nematic LCEs would be of especial importance due to their large deformation, reversible actuation, relative ease to manipulate and control, etc. So far, there has been no other report on using continuous fibers as the reinforcement phases for nematic LCE matrices. Polysiloxane-based nematic LCEs are generally synthesized by sol-gel method based on the procedure of two-stage crosslinking coupled with a drawing process [6], such synthesis process is suitable for the fabrication of large-sized LCE composite with flexile continuous fibers as reinforcement phase with a simple fabrication process and low cost. We developed a LCE nanocomposite with PUFN as the reinforcement phase and nematic LCE contained SWCNTs as the matrix. Not only attractive photo-responsive characteristic was demonstrated, but also the mechanical properties of photo auction were significantly enhanced. The effective load-actuation capability arrived 260 kPa which is very similar to that exhibited by skeletal muscles. In the future, we will improve the LCE nanocomposite for larger contraction ratio, lower threshold of response to the light, and higher loading capability.

References

[1] Chou, C. P., & Hannaford, B. (1996). *IEEE Trans. Robotics Automation.*, *12*, 90.

[2] Harris, K. D., Cuypers, R., Scheibe, P., van Oosten, C. L., Bastiaansen, C. W. M., Lub, J., & Broer, D. J. (2005). *J. Mater. Chem.*, *15*, 5043.
[3] Alexander, C., & Shakesheff, K. M. (2006). *Adv. Mater.*, *18*, 3321.
[4] Yu, H., & Ikeda, T. (2011). *Adv. Mater.*, *23*, 2149.
[5] Jiang, H., Li, C., & Huang, X. (2013). *Nanoscale.*, *5*, 5225.
[6] Warner, M., & Terentjev, E. M. (2003). *Liquid Crystal Elastomers*, Oxford University Press: Oxford.
[7] Yu, Y., Nakano, M., & Ikeda, T. (2003). *Nature.*, *425*, 145.
[8] Ikeda, T., Mamiya, J. I., & Yu, Y. (2007). *Angew. Chem.-Int. Edit.*, *46*, 506.
[9] Yang, H., Ye, G., Wang, X., & Keller, P. (2011). *Soft Matter.*, *7*, 815.
[10] Yang, H., Buguin, A., Taulemesse, J. M., Kaneko, K., Mery, S., Bergeret, A., & Keller, P. (2009). *J. Am. Chem. Soc.*, *131*, 15000.
[11] Ji, Y., Marshall, J. E., & Terentjev, E. M. (2012). *Polymers.*, *4*, 316.
[12] Camacho-Lopez, M., Finkelmann, H., Palffy-Muhoray, P., & Shelley, M. (2004). *Nat. Mater.*, *3*, 307.
[13] Van Oosten, C. L., Bastiaansen, C. W. M., & Broer, D. J. (2009). *Nat. Mater.*, *8*, 677.
[14] Serak, S., Tabiryan, N., Vergara, R., White, T. J., Vaia, R. A., & Bunning, T. J. (2010). *Soft Matter.*, *6*, 779.
[15] Yamada, M., Kondo, M., Mamiya, J., Yu, Y., Kinoshita, M., Barrett, C. J., & Ikeda, T. (2008). *Angew. Chem.-Int. Edit.*, *47*, 4986.
[16] Cheng, F., Yin, R., Zhang, Y., Yen, C. C., & Yu, Y. (2010). *Soft Matter.*, *6*, 3447.
[17] Chen, M., Xing, X., Liu, Z., Zhu, Y., Liu, H., Yu, Y., & Cheng, F. (2010). *Appl. Phys. A: Mater. Sci. Process.*, *100*, 39.
[18] Chen, M., Huang, H., Zhu, Y., Liu, Z., Xing, X., Cheng, F., & Yu, Y. (2011). *Appl. Phys. A: Mater. Sci. Process.*, *102*, 667.
[19] Kohlmeyer, R. R., & Chen, J. (2013). *Angew. Chem.-Int. Edit.*, *52*, 9234.
[20] Tang, R., Liu, Z. Y., Xu, D. D., Liu, J., Yu, L., & Yu, H. F. (2015). *ACS Appl. Mater. Interfaces.*, *7*, 8393.
[21] Xu, S., Ren, H., Lin, Y., Moharam, M. G. J., Wu, S., & Tabiryan, N. (2009). *Opt. Express.*, *17*, 17590.
[22] Yoshino, T., Kondo, M., Mamiya, J., Kinoshita, M., Yu, Y., & Ikeda, T. (2010). *Adv. Mater.*, *22*, 1361.
[23] Li, C., Lo, C. W., Li, C., Zhu, D., Liu, Y., & Jiang, H. (2009). *Macromol. Rapid Commun.*, *30*, 1928.
[24] Yu, H., Dong, C., Zhou, W., Kobayashi, T., & Yang, H. (2011). *Small.*, *7*, 3039.
[25] Yu, H. (2014). *J. Mater. Chem. C.*, *2*, 3047.
[26] Yang, L., Setyowati, K., Li, A., Gong, S., & Chen, J. (2008). *Adv. Mater.*, *20*, 2271.
[27] Ji, Y., Huang, Y., Rungsawang, R., & Terentjev, E. M. (2010). *Adv. Mater.*, *22*, 3436.
[28] Li, C., Liu, Y., Lo, C. W., & Jiang, H. R. (2011). *Soft Matter.*, *16*, 7511.
[29] Marshall, J. E., Ji, Y., Torras, N., Zinoviev, K., & Terentjev, E. M. (2012). *Soft Matter.*, *8*, 1570.
[30] Li, C., Liu, Y., Huang, X., & Jiang, H. (2012). *Adv. Funct. Mater.*, *22*, 5166.
[31] Tajbakhsh, A. R., & Terentjev, E. M. (2001). *Eur. Phys. J. E.*, *6*, 181.
[32] Robert, M. J. (1975). *Mechanics of Composite Materials*, McGraw-Hill Book Company: New York.
[33] Courty, S., Mine, J., Tajbakhsh, A. R., & Terentjev, E. M. (2003). *Europhys. Lett.*, *64*, 654.
[34] Wang, W., Sun, X., Wu, W., Peng, H., & Yu, Y. (2012). *Angew. Chem. Int. Ed.*, *51*, 4644.
[35] Naka, Y., Mamiya, J., Shishido, A., Washio, M., & Ikeda, T. (2011). *J. Mater. Chem.*, *21*, 1681.
[36] Agrawal, A., Yun, T. H., Pesek, S. L., Chapman, W. G., & Verduzco, R. (2014). *Soft Matter.*, *10*, 1411.
[37] Greve, A., & Finkelmann, H. (2001). *Macromol. Chem. Phys.*, *202*, 2926.